Regular Article

Performance Analysis of CR-NOMA Network with Active RIS-Enhanced Systems

Hong-Nhu Nguyen*, Ngoc Thuy Trang Nguyen, Hai Sinh Chu, Nguyen Minh Quan Bui

Faculty of Engineering and Technology, Saigon University (SGU), Ho Chi Minh City, Vietnam

Correspondence: Hong-Nhu Nguyen*, nhu.nh@sgu.edu.vn
Communication: received 12 February 2025, revised 08 April 2025, accepted 25 May 2025
Online publication: 02 June 2025, Digital Object Identifier: 10.21553/rev-jec.396

Abstract– **This paper proposes a reconfigurable intelligent surface (RIS)-assisted underlay spectrum sharing system, in which a RIS-assisted secondary network shares the spectrum licensed for a primary network. The secondary network consists of a secondary source (BS), an RIS, and a secondary destination (SD), operating in a Rician fading environment. We study the performance of the secondary network while considering a peak power constraint at the BS and an interference power constraint at the primary receiver (PR). Building upon the SNR statistics, we analyze the outage probability and throughput, deriving novel exact expressions for these performance measures. Finally, we conduct exhaustive Monte-Carlo simulations to confirm the correctness of our theoretical analysis.**

Keywords– **NOMA, active-RIS, spectrum sharing, 6G wireless communications, outage probability.**

1 Introduction

The 6G is a technology trend to expand networking coverage to allow a tremendous number of subscribers and congested regions of small devices to be connected efficiently and with unconventionally high data rate speeds. The random nature of fading environments and the disruptive interactions of the propagated waves with the adjacent objects are the main causes of signal degradation in wireless communication systems. The technology of reconfigurable intelligent surfaces (RISs) has been designed to allow network operators to control reflection, refraction, and scattering characteristics of propagated radio waves in a manner yielding to reducing the negative impacts of fading environments and improving received signals quality.

RIS is a promising technology to enhance the coverage and performance of wireless networks. In [1], the authors investigated the application of RIS to non-orthogonal multiple access (NOMA) with cognitive radio. The paper considered the performance of active RIS (ARIS) with a sub-connected architecture, decoupling the RIS reflection coefficients optimization into amplification factor and phase shift subproblems to be solved separately for energy efficiency. At the same time, it validates the effectiveness of the proposed schemes and demonstrates the weakness of passive RIS (PRIS). The performance of an RIS-assisted NOMA network with secondary source controls the information transmission to two secondary users via the ARIS element. This paper evaluates critical system performance indicators such as outage probability, achievable ergodic rate, throughput, and energy efficiency. Besides, the authors evaluated the results and compared between ARIS and PRIS schemes [2, 3]. In [4], B. Zheng et al. have provided a comprehensive survey on the up-to-date research in RIS-aided wireless communications, with an emphasis on promising solutions to tackle practical design issues. The author group has investigated the secure communications of RIS-assisted NOMA networks, where both external and internal eavesdropping scenarios are taken into consideration [5]. The secrecy system throughput of RIS-NOMA networks is discussed in delay-limited transmission mode [6].

Internet of Things (IoT) systems have been implemented for over a decade, from transportation to military surveillance, and are proven worthy of integration in the next generation of wireless protocols [7]. To overcome these challenges, the integration of IoT with spectrum-efficient techniques, including cognitive radio (CR) and NOMA has been proposed [8]. NOMA is viewed as a viable candidate to increase connectivity and spectral effectiveness over traditional methods in emerging wireless networks by exploiting SIC and superposition coding to enable more user connectivity with no interference. Active RIS is a promising way to compensate for multiplicative fading attenuation by amplifying and reflecting event signals to selected users. The authors in [9] have investigated the performance of combined active reconfigurable intelligent surface (ARIS) and NOMA networks to provide strengthened outage performance.

To the best of the authors' knowledge, although the aforementioned studies have extensively investigated the performance of CR-NOMA and ARIS-assisted. In which they considered energy efficiency, ergodic rate and system security. In this work, we propose a system model while simultaneously analyzing the system's performance through comparison between ARIS

and PRIS. Additionally, the channel is modeled using a generalized Nakagami-m fading distribution. The main contributions of this paper are as follows:

- We propose a system model CR-NOMA with RIS-assisted to improve the performance of system.
- Based on RIS comparison, we evaluated two important metrics such as OP and throughput. Simultaneously, we are compare ARIS, PRIS in the cases NOMA and OMA technology.
- We provide closed-form expressions of OP based on SINR computed to detect signals. In addition, we apply algorithms founded on the golden section search method to ascertain the precise value of power allocation factors that minimize the outage probability for the second user.

Organization: The subsequent sections of this manuscript are organized as follows. Section II delineates the system architecture of ARIS-assisted NOMA spectrum-sharing communications. The exact and approximate outage probabilities pertinent to ARIS-NOMA spectrum-sharing networks are meticulously delineated in Section III. The numerical evaluations are presented in Section IV. Lastly, Section V encapsulates the findings of this manuscript. The mathematical proofs are compiled in the appendix.

Notation: The important notations in this work are shown here. The symbol $(\cdot)^H$ indicates the conjugate transpose operation. $\Pr(.)$ denotes the probability operator; $\mathbb{E}\{.\}$ and $\mathbb{D}\{.\}$ denote the expectation and variance operations, respectively; $H(x)$ is so-called the Heaviside step function; $\Gamma(a)$ is the Gamma function; $\Gamma(.,.)$ denotes the upper incomplete gamma function; $G_{p,q}^{m,n}[.]$ is the Meijer G-function; the probability density function (PDF) and the cumulative distribution function (CDF) of a random variable X are represented as $F_X(.)$ and $f_X(.)$, respectively. The symbol $\mathrm{diag}(\cdot)$ represents a diagonal matrix with only one member.

2 System Model

2.1 System Description

We examine a communication scenario involving RIS-assisted NOMA spectrum sharing, illustrated in Figure 1, where a primary network includes a primary user (PU) equipped with a single antenna. The secondary network consists of a single antenna base station (BS) serving two single antenna users (the nearby user U_1 and the more distant user U_2) through N active reflecting elements. Specifically, contemporary ARIS architectures not only feature identical circuitry for phase shift control as seen in PRIS, but also incorporate power amplifiers to enhance the transmitted signal. The incident superimposed signals at ARIS are boosted with a noticeable gain before being reflected towards the intended users. The inherent multiplicative attenuation present in PRIS-assisted systems will be effectively addressed by active elements while maintaining low power consumption. In articles published, the authors

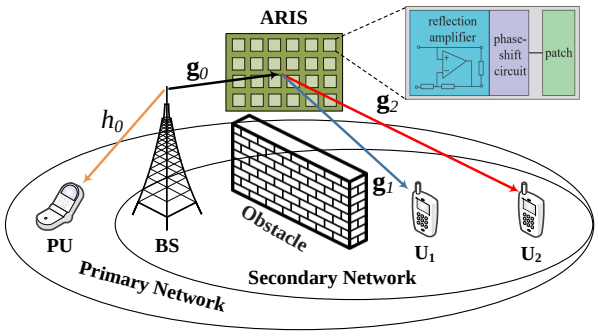

Figure 1. The system model of RIS-assisted communications.

studied the direct links between BS and users that are hindered by high-rise buildings [1], where the implementation of ARIS can establish a line-of-sight between the BS and non-orthogonal users. Distortions on both the BS and users' sides are taken into account to more accurately reflect real-world scenarios.

To represent genuine channel circumstances, we assume that the wireless connections of ARIS-NOMA networks undergo large-scale fading and Nakagami-m fading [1]. We use o denote the channel coefficient from the BS to the PU. Let $\mathbf{g}_i = \left[g_i^1, \ldots, g_i^n, \ldots g_i^N\right]^H$, $i \in \{1,2\}$ and $\mathbf{g}_0 = \left[g_0^1, \ldots, g_0^n, \ldots g_0^N\right]^H$ represent the baseband channel coefficients between ARIS and U_i and BS to the ARIS. g_0^n and g_i^n represent the complicated channel factors that exist between BS and ARIS's nth reflective element, as well as between ARIS's nth reflective element and user i, respectively. The reflection matrix at ARIS is specified as $\mathbf{\Phi} = \sqrt{\beta}\mathrm{diag}\left(e^{j\theta_1}, \ldots, e^{j\theta_n}, \ldots e^{j\theta_N}\right)$, where the angle θ_n lies within the interval ranging from 0 to 2π, and the variable β signifies the phase shift associated with the nth reflection element along with its corresponding reflection amplification coefficient. The reflection elements integrated within ARIS are strategically situated within active amplifiers that utilize either tunneling diodes or resistive converters, thereby enhancing their operational capabilities. Leveraging the fundamental principles of electromagnetic scattering, each individual element is capable of not only reflecting an incoming radio frequency (RF) signal but also amplifying it, with both the amplitude and phase being adjustable to meet specific requirements. This sophisticated feature enables ARIS to attain a reflection amplification coefficient that exceeds unity, which mathematically translates to β being greater than 1, as referenced in numerous studies [2, 3]. In practical implementations, a negative resistive element, such as a tunnel diode, can be effectively employed to amplify the incident RF signal, facilitating the conversion of direct current bias power into RF power, thereby enhancing the performance of the system. As a result, the integration of such components allows for a remarkable

[1]It is worth noting that the derivations of performance analyses specifically designed for ARIS-aided NOMA spectrum sharing networks can be easily and seamlessly applied across a wide range of multiple fading channels, i.e., the Gaussian fading channel, the Rayleigh fading channel, and the Rician fading channel.

increase in signal strength and quality, which is crucial for advanced communication and imaging applications. Consequently, the innovative design and functionality of ARIS play a pivotal role in advancing the field of radio frequency technology and its myriad applications in both research and industry. We assume that the instantaneous channel state information (CSI) is available at both the BS and ARIS through the use of channel estimation or compressive sensing techniques [4]. This paper does not address the imperfect CSI that affects the performance of ARIS-NOMA networks.

2.2 Channel Model

In spectrum-sharing systems, the PU requires that the instantaneous interference caused by the BS be less than a set threshold Q, which represents the maximum permitted interference power at the PU. At the same time, the BS' transmit power is limited by a peak power restriction. As a result, the transmit power at the base station may be stated as

$$P_b = \min\left(\bar{P}_b, \frac{Q}{|h_0|^2}\right), \tag{1}$$

where the maximum power of the BS is $\bar{P}_b$, and Q is the interference temperature constraint (ITC) at PU.

The BS transfers superimposed signals, i.e., $x = \sqrt{a_1 P_b}x_1 + \sqrt{a_2 P_b}x_2$, specifically directed towards user i through a process known as ARIS, where the parameters x_1 and x_2 are defined as normalized power signals that maintain a unity value for U_1 and U_2, respectively, ensuring that both users receive the appropriate signal strength. To ensure non-orthogonal users' fairness, the power allocation factors a_1 and a_2 for U_1 and U_2 must meet the relations $a_1 < a_2$ and $a_1 + a_2 = 1$. P_b represents the BS transmission power. Unlike PRIS, ARIS uses active devices such as tunnel or Gunn diodes to enhance overlaid signals and noise received at itself. In these situations, the received signals at user i, $(i \in \{1, 2\})$ can be described as

$$y_i = \sqrt{\beta}\mathbf{g}_i^H \mathbf{\Theta}\mathbf{g}_0 x + \sqrt{\beta}\mathbf{g}_i^H \mathbf{\Theta}\mathbf{n}_0 + \omega_i, \tag{2}$$

where $\mathbf{\Theta} = \text{diag}\left(e^{j\theta_1}, \ldots, e^{j\theta_n}, \ldots e^{j\theta_N}\right)$ is so-called the phase shift matrix at ARIS. $\mathbf{n}_0 \sim \mathcal{CN}\left(0, N_{tn}\mathbf{I}_N\right)$ denotes the thermal noise at ARIS with the noise power N_{tn} and $\mathbf{I}_N \in \mathbb{C}^{N\times 1}$ is the identity matrix. ω_i indicates the Gaussian white noise generated at the user i with $\omega_i \sim \mathcal{CN}\left(0, \sigma^2\right)$.

In accordance with the NOMA principle, U_1 initially identifies U_2's information, which has superior channel conditions, and subsequently removes it before decoding its signal. Therefore, the resultant received SINR can be expressed as

$$\begin{aligned}\gamma_{x_2\to x_1} =& \frac{\beta P_b a_2 \left|\mathbf{g}_1^H \mathbf{\Theta}\mathbf{g}_0\right|^2}{\beta P_b a_1 \left|\mathbf{g}_1^H \mathbf{\Theta}\mathbf{g}_0\right|^2 + \xi\beta N_{tn}\left|\mathbf{g}_1^H \mathbf{\Theta}\right|^2 + \sigma^2} \\ =& \frac{\beta \rho_b a_2 \left|\mathbf{g}_1^H \mathbf{\Theta}\mathbf{g}_0\right|^2}{\beta \rho_b a_1 \left|\mathbf{g}_1^H \mathbf{\Theta}\mathbf{g}_0\right|^2 + \xi\beta N_{tn}\left|\mathbf{g}_1^H \mathbf{\Theta}\right|^2 + 1},\end{aligned} \tag{3}$$

here $\rho_b = P_b/\sigma^2$ represents the transmit signal-to-noise ratio (SNR), while ξ is the conversion factor. Within ARIS networks, ξ is assigned a value of 1. To be more specific, if ξ is zero, ARIS transforms into PRIS. After eliminating the information from U_2, the receiving SINR for U_1, while decoding its own signal, can be expressed as

$$\gamma_{x_1} = \frac{\beta \rho_b a_1 \left|\mathbf{g}_1^H \mathbf{\Theta}\mathbf{g}_0\right|^2}{\xi\beta N_{tn}\left|\mathbf{g}_1^H \mathbf{\Theta}\right|^2 + 1}. \tag{4}$$

Under channel conditions U_2, identifies x_1 as interference and thus directly determines its signal x_2. For now, the SINR that U_2 uses to detect x_2 can be expressed as

$$\gamma_{x_2} = \frac{\beta \rho_b a_2 \left|\mathbf{g}_2^H \mathbf{\Theta}\mathbf{g}_0\right|^2}{\beta \rho_b a_1 \left|\mathbf{g}_2^H \mathbf{\Theta}\mathbf{g}_0\right|^2 + \xi\beta N_{tn}\left|\mathbf{g}_2^H \mathbf{\Theta}\right|^2 + 1}. \tag{5}$$

To demonstrate the performance advantages of ARIS-NOMA, we use ARIS-OMA as a to demonstrate the performance advantages of ARIS-NOMA, we use ARIS-OMA as a benchmark for comparison. We have the SINR for user O is provided by

$$\gamma_O = \frac{\beta \rho_b \left|\mathbf{g}_O^H \mathbf{\Theta}\mathbf{g}_0\right|^2}{\xi\beta N_{tn}\left|\mathbf{g}_O^H \mathbf{\Theta}\right|^2 + 1}. \tag{6}$$

where $\mathbf{g}_O = \left[h_O^1, h_O^2, \ldots, h_O^n, \ldots, h_O^N\right]^H$ denotes the complex channel coefficient between ARIS and user O.

3 Outage Probability

In this segment, we evaluate the performance of ARIS-NOMA/OMA secondary networks by scrutinizing their outage characteristics, wherein we formulate the closed-form expressions for outage probabilities pertaining to U_1 and U_2 within the framework of cascade Nakagami-m fading channels. Additionally, we consider the thermal noise produced by ARIS to be a constant in facilitating the computational analysis.

3.1 The Outage Probability of U_1

In this scenario, the occurrence of outage behavior at U_1 transpires when U_1 is unable to perceive the signal from U_2 as well as its own signal. We may articulate such an adverse situation as follows

$$\begin{aligned}\mathcal{P}_{U_1}^{ARIS} =& 1 - \Pr\left(\min\left(\frac{\gamma_{x_2\to x_1}}{\gamma_{th_2}}, \frac{\gamma_{x_1}}{\gamma_{th_1}}\right) < 1\right) \\ =& 1 - \Pr\left(\gamma_{x_2\to x_1} > \gamma_{th_2}, \gamma_{x_1} > \gamma_{th_1}\right),\end{aligned} \tag{7}$$

here $\gamma_{th_1} = 2^{R_1} - 1$ and $\gamma_{th_2} = 2^{R_2} - 1$ denote the desired SNRs at U_1 for decoding x_1 and x_2, respectively. R_1 and R_2 represent the corresponding goal rates.

Proposition 1: With respect to cascade Nakagami-m fading channels, the closed-form for the outage probability of U_1 within ARIS-NOMA spectrum-sharing

$$\Lambda(a,b,c) = H_{2,1:0,1:1,1}^{0,2:1,0:0,1}\left(\begin{array}{c|c|c} (-a-2m_0;2,1),(1-2m_0;2,1) & - & (1,1) \\ (-2m_0;2,1) & (0,1) & (0,1) \end{array} \middle| b,c \right). \tag{9}$$

networks can be given as

$$\mathcal{P}_{U_1}^{ARIS} = 1 - \left[1 - e^{-\frac{\mu_0\rho_Q}{\bar{\rho}_b}} \sum_{t=0}^{m_0-1} \frac{\mu_0^t \rho_Q^t}{t!\bar{\rho}_b^t}\right] \frac{\Gamma\left(b_1+1, c_1^{-1}\sqrt{\frac{\phi_{\max} d_1}{\bar{\rho}_b}}\right)}{\Gamma(b_1+1)} - \frac{2\mu_0^{m_0}\vartheta_1^{-2m_0}}{\Gamma(m_0)\Gamma(b_1+1)} \Lambda\left(b_1, \frac{\mu_0}{\vartheta_1^2}, \frac{1}{\vartheta_1}\sqrt{\frac{\bar{\rho}_b}{\rho_Q}}\right), \tag{8}$$

where $\phi_2 = \frac{\gamma_{th_2}}{\beta\left(a_2 - \gamma_{th_2} a_1\right)}$, $\phi_1 = \frac{\gamma_{th_1}}{\beta a_1}$, $\phi_{\max} = \max(\phi_1, \phi_2)$, $d_1 = \xi\beta N_{tn}\Omega_1 + 1$, $\vartheta_1 = c_1^{-1}\sqrt{\frac{\phi_{\max} d_1}{\rho_Q}}$ $\mu_0 = \frac{m_{h_0}}{\lambda_{h_0}}$, $b_1 = \frac{N\mu_1^2}{\Omega_1} - 1$, $c_1 = \frac{\Omega_1}{\mu_1}$, $\mu_1 = \frac{\Gamma\left(m_{g_0}+0.5\right)\Gamma\left(m_{g_1}+0.5\right)\sqrt{\lambda_{g_0}\lambda_{g_1}}}{\Gamma\left(m_{g_0}\right)\Gamma\left(m_{g_1}\right)\sqrt{m_{g_0} m_{g_1}}}$, $\Omega_1 = \lambda_{g_0}\lambda_{g_1}\left\langle 1 - \frac{1}{m_{g_0} m_{g_1}}\left[\frac{\Gamma\left(m_{g_0}+0.5\right)\Gamma\left(m_{g_1}+0.5\right)}{\Gamma\left(m_{g_0}\right)\Gamma\left(m_{g_1}\right)}\right]^2\right\rangle$. We have m_{h_0}, m_{g_0} and m_{g_1} denote the Nakagami-m fading parameters from the BS−PU, BS−ARIS and ARIS−U_1, respectively. $\lambda_{h_0} = \mathbb{E}\left\{|h_0|^2\right\}$, $\lambda_{g_0} = \mathbb{E}\left\{\left|g_0^n\right|^2\right\}$ and $\lambda_{g_1} = \mathbb{E}\left\{\left|g_1^n\right|^2\right\}$ are the mean of $|h_0|^2$, $\left|g_0^n\right|^2$ and $\left|g_1^n\right|^2$, respectively. We have $\mathbb{E}\{.\}$ and $\Gamma(.)$ represent the the expectation operation and the gamma function, respectively. $\Gamma(.,.)$ denotes the upper incomplete gamma function. $\mathcal{H}_{p,q:u,v:e,f}^{m,n:s,t:i,j}(\cdot)$ represents the extended generalized bivariate Fox H-function (EGBFHF) in [5] and $\Lambda(a,b,c)$ is shown on the top page.

Proof: See Appendix A.

When $\xi = 0$, the closed-form outage probability of U_1 for PRIS-NOMA may be stated as

$$\mathcal{P}_{U_1}^{PRIS} = 1 - \left[1 - e^{-\frac{\mu_0\rho_Q}{\bar{\rho}_b}} \sum_{t=0}^{m_0-1} \frac{\mu_0^t \rho_Q^t}{t!\bar{\rho}_b^t}\right] \frac{\Gamma\left(b_1+1, c_1^{-1}\sqrt{\bar{\rho}_b^{-1}\bar{\phi}_{\max}}\right)}{\Gamma(b_1+1)} - \frac{2\mu_0^{m_0}\bar{\vartheta}_1^{-2m_0}}{\Gamma(m_0)\Gamma(b_1+1)} \Lambda\left(b_1, \frac{\mu_0}{\bar{\vartheta}_1^2}, \frac{1}{\bar{\vartheta}_1}\sqrt{\frac{\bar{\rho}_b}{\rho_Q}}\right), \tag{10}$$

where $\bar{\phi}_2 = \frac{\gamma_{th_2}}{a_2 - \gamma_{th_2} a_1}$, $\bar{\phi}_1 = \frac{\gamma_{th_1}}{a_1}$, $\bar{\phi}_{\max} = \max(\bar{\phi}_1, \bar{\phi}_2)$ and $\bar{\vartheta}_1 = c_1^{-1}\sqrt{\frac{\bar{\phi}_{\max}}{\rho_Q}}$.

3.2 The Outage Probability of U_2

Concerning U_2 facing deteriorated channel conditions, an interruption is initiated if it cannot recognize or decode its transmitted message x_2. In such circumstances, the outage probability for U_2 within the context of ARIS-NOMA spectrum-sharing networks is defined by

$$\begin{aligned} \mathcal{P}_{U_2}^{ARIS} &= \Pr\left(\gamma_{x_2} < \gamma_{th_2}\right) \\ &= 1 - \Pr\left(\gamma_{x_2} > \gamma_{th_2}\right) \\ &= 1 - \mathcal{B}_1 - \mathcal{B}_2, \end{aligned} \tag{11}$$

where $\mathcal{B}_1$ and $\mathcal{B}_1$ are already given as

$$\mathcal{B}_1 = \Pr\left(\begin{array}{l} \left|\mathbf{g}_2^H \boldsymbol{\Theta} \mathbf{g}_0\right|^2 > \frac{\phi_2}{\bar{\rho}_b}\left(\xi\beta N_{tn}\left|\mathbf{g}_2^H\boldsymbol{\Theta}\right|^2 + 1\right) \\ |h_0|^2 < \frac{\rho_Q}{\bar{\rho}_b} \end{array} \right), \tag{12a}$$

$$\mathcal{B}_2 = \Pr\left(\begin{array}{l} \left|\mathbf{g}_2^H \boldsymbol{\Theta} \mathbf{g}_0\right|^2 > \frac{\phi_2|h_0|^2}{\rho_Q}\left(\xi\beta N_{tn}\left|\mathbf{g}_2^H\boldsymbol{\Theta}\right|^2 + 1\right) \\ |h_0|^2 > \frac{\rho_Q}{\bar{\rho}_b} \end{array} \right). \tag{12b}$$

Similarly, by solving $\mathcal{P}_{U_1}^{ARIS}$ and the closed-form of the outage probability for U_2 within ARIS-NOMA spectrum-sharing networks may be articulated as

$$\mathcal{P}_{U_2}^{ARIS} = 1 - \left[1 - e^{-\frac{\mu_0\rho_Q}{\bar{\rho}_b}} \sum_{t=0}^{m_0-1} \frac{\mu_0^t \rho_Q^t}{t!\bar{\rho}_b^t}\right] \frac{\Gamma\left(b_2+1, c_2^{-1}\sqrt{\frac{\phi_2 d_2}{\bar{\rho}_b}}\right)}{\Gamma(b_2+1)} - \frac{2\mu_0^{m_0}\vartheta_2^{-2m_0}}{\Gamma(m_0)\Gamma(b_2+1)} \Lambda\left(b_2, \frac{\mu_0}{\vartheta_2^2}, \frac{1}{\vartheta_2}\sqrt{\frac{\bar{\rho}_b}{\rho_Q}}\right), \tag{13}$$

where $d_2 = \xi\beta N_{tn}\Omega_2 + 1$ and $\vartheta_2 = c_2^{-1}\sqrt{\frac{\phi_2 d_2}{\rho_Q}}$.

When parameter ξ is set to zero, the closed-form outage probability of U_2 for PRIS-NOMA may be stated as

$$\mathcal{P}_{U_2}^{PRIS} = 1 - \left[1 - e^{-\frac{\mu_0\rho_Q}{\bar{\rho}_b}} \sum_{t=0}^{m_0-1} \frac{\mu_0^t \rho_Q^t}{t!\bar{\rho}_b^t}\right] \frac{\Gamma\left(b_2+1, c_2^{-1}\sqrt{\bar{\rho}_b^{-1}\bar{\phi}_2}\right)}{\Gamma(b_2+1)} - \frac{2\mu_0^{m_0}\bar{\vartheta}_2^{-2m_0}}{\Gamma(m_0)\Gamma(b_2+1)} \Lambda\left(b_2, \frac{\mu_0}{\bar{\vartheta}_2^2}, \frac{1}{\bar{\vartheta}_2}\sqrt{\frac{\bar{\rho}_b}{\rho_Q}}\right), \tag{14}$$

where $\bar{\vartheta}_2 = c_2^{-1}\sqrt{\frac{\bar{\phi}_2}{\rho_Q}}$.

3.3 The Outage Probability of User O

In a manner similar to the aforementioned analytical advancements, the probability of outage for orthogonal user O within ARIS-OMA spectrum-sharing networks is articulated as by

$$\mathcal{P}_O^{ARIS} = 1 - \Pr\left(\gamma_O > \gamma_{th_O}\right). \tag{15}$$

where γ_{th_O} denotes the target SNRs of user O.

Subject to the constraints of cascade Nakagami-m fading channels, the outage probability associated with user O within ARIS-OMA spectrum-sharing networks may be articulated as

$$\mathcal{P}_O^{ARIS} = 1 - \left[1 - e^{-\frac{\mu_0\rho_Q}{\bar{\rho}_b}} \sum_{t=0}^{m_0-1} \frac{\mu_0^t \rho_Q^t}{t!\bar{\rho}_b^t}\right] \frac{\Gamma\left(b_O+1, c_O^{-1}\sqrt{\frac{\phi_O d_O}{\bar{\rho}_b}}\right)}{\Gamma(b_O+1)} - \frac{2\mu_0^{m_0}\vartheta_O^{-2m_0}}{\Gamma(m_0)\Gamma(b_O+1)} \Lambda\left(b_O, \frac{\mu_0}{\vartheta_O^2}, \frac{1}{\vartheta_O}\sqrt{\frac{\bar{\rho}_b}{\rho_Q}}\right), \tag{16}$$

where $\phi_O = \frac{\gamma_{th_O}}{\beta}$, $d_O = \xi\beta N_{tn}\Omega_O + 1$ and $\vartheta_O = c_O^{-1}\sqrt{\frac{\phi_O d_O}{\rho_Q}}$.

When the parameter ξ is set to be zero, the closed-form outage probability of user O for PRIS-OMA can be expressed as

$$\mathcal{P}_O^{PRIS} = 1 - \left[1 - e^{-\frac{\mu_0\rho_Q}{\bar{\rho}_b}} \sum_{t=0}^{m_0-1} \frac{\mu_0^t \rho_Q^t}{t!\bar{\rho}_b^t}\right] \frac{\Gamma\left(b_O+1, c_O^{-1}\sqrt{\frac{\gamma_{th_O}}{\bar{\rho}_b}}\right)}{\Gamma(b_O+1)} - \frac{2\mu_0^{m_0}\bar{\vartheta}_O^{-2m_0}}{\Gamma(m_0)\Gamma(b_O+1)} \Lambda\left(b_O, \frac{\mu_0}{\bar{\vartheta}_O^2}, \frac{1}{\bar{\vartheta}_O}\sqrt{\frac{\bar{\rho}_b}{\rho_Q}}\right), \tag{17}$$

where $\bar{\vartheta}_O = c_O^{-1}\sqrt{\frac{\gamma_{th_O}}{\rho_Q}}$.

3.4 Diversity Analysis

In this segment, we select the diversity order to scrutinize the outage characteristics of ARIS-NOMA spectrum-sharing networks. In other terms, the diversity order serves to characterize the rate at which the likelihood of outage diminishes as the SNR increases [6]. As the diversity order is enhanced, the probability of outage declines more rapidly. To elaborate further, the diversity order is articulated as

$$\mathcal{D} = -\lim_{\bar{\rho}_b\to\infty} \frac{\log\left(\mathcal{P}^{\infty}\left(\bar{\rho}_b\right)\right)}{\log\left(\bar{\rho}_b\right)}, \tag{18}$$

where $\mathcal{P}^{\infty}\left(\bar{\rho}_b\right)$ represents the asymptotic outage probability in case of high SNRs.

When $\bar{\rho}_b$ goes to infinity then we have $\mathcal{A}_1 \approx 0$ and $\frac{\rho_Q}{\bar{\rho}_b} \approx 0$, the asymptotic expression for $\mathcal{P}_{U_1}^{ARIS,\infty}$ is calculated as

$$\begin{aligned}\mathcal{P}_{U_1}^{ARIS,\infty} &= \Pr\left(\left|\sum_{n=1}^{N} g_0^n g_1^n\right| > \sqrt{\frac{\phi_{\max} d_1 |h_0|^2}{\rho_Q}}, |h_0|^2 > 0\right) \\ &= 1 - \frac{\mu_0^{m_0}}{\Gamma\left(m_0\right)\Gamma\left(b_1+1\right)} \int_0^{\infty} x^{m_0-1} e^{-\mu_0 x} \\ &\quad \times \Gamma\left(b_1+1, \vartheta_1\sqrt{x}\right) dx.\end{aligned} \tag{19}$$

Let $t = \sqrt{x}$ and rewriting the exponential term with the G-function, (19) is rewritten as follows

$$\begin{aligned}\mathcal{P}_{U_1}^{ARIS,\infty} &= 1 - \frac{2\mu_0^{m_0}}{\Gamma\left(m_0\right)\Gamma\left(b_1+1\right)} \int_0^{\infty} t^{2m_0-1} e^{-\mu_0 t^2} \\ &\quad \times \Gamma\left(b_1+1, \vartheta_1 t\right) dt \\ &= 1 - \frac{2\mu_0^{m_0}}{\Gamma\left(m_0\right)\Gamma\left(b_1+1\right)} \int_0^{\infty} t^{2m_0-1} \\ &\quad \times G_{1,2}^{2,0}\left(\vartheta_1 t \,\middle|\, \begin{matrix} 1 \\ b_1+1, 0 \end{matrix}\right) G_{0,1}^{1,0}\left(\mu_0 t^2 \,\middle|\, \begin{matrix} - \\ 0 \end{matrix}\right) dt.\end{aligned} \tag{20}$$

Using property [[7], Equation (2.24)], the asymptotic outage probability of U_1 for ARIS-NOMA may be calculated as follows

$$\mathcal{P}_{U_1}^{ARIS,\infty} = 1 - \frac{2^{b_1+0.5+2m_0}\mu_0^{m_0}\vartheta_1^{-2m_0}}{\sqrt{2\pi}\Gamma\left(m_0\right)\Gamma\left(b_1+1\right)} \times G_{4,3}^{1,4}\left(\frac{4\mu_0}{\vartheta_1^2} \,\middle|\, \begin{matrix} \frac{-b_1-2m_0}{2}, \frac{1-b_1-2m_0}{2}, \frac{1-2m_0}{2}, 1-m_0 \\ 0, -m_0, \frac{1-2m_0}{2} \end{matrix}\right). \tag{21}$$

When ξ equals zero, the asymptotic outage probability of U_1 for PRIS-NOMA may be calculated as

$$\mathcal{P}_{U_1}^{PRIS,\infty} = 1 - \frac{2^{b_1+0.5+2m_0}\mu_0^{m_0}\bar{\vartheta}_1^{-2m_0}}{\sqrt{2\pi}\Gamma\left(m_0\right)\Gamma\left(b_1+1\right)} \times G_{4,3}^{1,4}\left(\frac{4\mu_0}{\bar{\vartheta}_1^2} \,\middle|\, \begin{matrix} \frac{-b_1-2m_0}{2}, \frac{1-b_1-2m_0}{2}, \frac{1-2m_0}{2}, 1-m_0 \\ 0, -m_0, \frac{1-2m_0}{2} \end{matrix}\right). \tag{22}$$

As $\bar{\rho}_b$ approaches infinity, the asymptotic outage probability of U_2 for ARIS/PRIS-NOMA may be calculated by

$$\mathcal{P}_{U_2}^{ARIS,\infty} = 1 - \frac{2^{b_1+0.5+2m_0}\mu_0^{m_0}\vartheta_2^{-2m_0}}{\sqrt{2\pi}\Gamma\left(m_0\right)\Gamma\left(b_1+1\right)} \times G_{4,3}^{1,4}\left(\frac{4\mu_0}{\vartheta_2^2} \,\middle|\, \begin{matrix} \frac{-b_1-2m_0}{2}, \frac{1-b_1-2m_0}{2}, \frac{1-2m_0}{2}, 1-m_0 \\ 0, -m_0, \frac{1-2m_0}{2} \end{matrix}\right), \tag{23}$$

and

$$\mathcal{P}_{U_2}^{PRIS,\infty} = 1 - \frac{2^{b_1+0.5+2m_0}\mu_0^{m_0}\bar{\vartheta}_2^{-2m_0}}{\sqrt{2\pi}\Gamma\left(m_0\right)\Gamma\left(b_1+1\right)} \times G_{4,3}^{1,4}\left(\frac{4\mu_0}{\bar{\vartheta}_2^2} \,\middle|\, \begin{matrix} \frac{-b_1-2m_0}{2}, \frac{1-b_1-2m_0}{2}, \frac{1-2m_0}{2}, 1-m_0 \\ 0, -m_0, \frac{1-2m_0}{2} \end{matrix}\right). \tag{24}$$

Similarly, by solving (23) and (24), the asymptotic outage probability of user O for ARIS-OMA and PRIS-OMA can be separately expressed as

$$\mathcal{P}_O^{ARIS,\infty} = 1 - \frac{2^{b_1+0.5+2m_0}\mu_0^{m_0}\vartheta_O^{-2m_0}}{\sqrt{2\pi}\Gamma\left(m_0\right)\Gamma\left(b_O+1\right)} \times G_{4,3}^{1,4}\left(\frac{4\mu_0}{\vartheta_O^2} \,\middle|\, \begin{matrix} \frac{-b_O-2m_0}{2}, \frac{1-b_O-2m_0}{2}, \frac{1-2m_0}{2}, 1-m_0 \\ 0, -m_0, \frac{1-2m_0}{2} \end{matrix}\right), \tag{25}$$

and

$$\mathcal{P}_O^{PRIS,\infty} = 1 - \frac{2^{b_1+0.5+2m_0}\mu_0^{m_0}\bar{\vartheta}_O^{-2m_0}}{\sqrt{2\pi}\Gamma\left(m_0\right)\Gamma\left(b_O+1\right)} \times G_{4,3}^{1,4}\left(\frac{4\mu_0}{\bar{\vartheta}_O^2} \,\middle|\, \begin{matrix} \frac{-b_O-2m_0}{2}, \frac{1-b_O-2m_0}{2}, \frac{1-2m_0}{2}, 1-m_0 \\ 0, -m_0, \frac{1-2m_0}{2} \end{matrix}\right). \tag{26}$$

Upon substituting equations (26), (25), (24), (23), (22), and (21) into equation (18), it is observed that the diversity order of user Z, $Z \in \{U_1, U_2, O\}$ is equivalent to zero. This phenomenon arises from the residual interference induced by the temperature constraint at the PU. We see that diversity order is the power exponent, which defines the rate of convergence of Pb to the error floor. Furthermore, it can be deduced that the diversity order is linked to the number of reflected elements and the order of the channels, and it is noteworthy that the introduction of thermal noise from the ARIS does not influence the diversity order.

3.5 Delay-Limited Transmission

In delay-limited systems, the BS transmits data at a consistent rate, which is affected by the stochastic variations of the wireless channel. The resultant system

throughput can be expressed as [9]

$$\tau^{\star} = \left(1 - \mathcal{P}^{\star}_{U_1}\right) R_1 + \left(1 - \mathcal{P}^{\star}_{U_2}\right) R_2, \star \in \{ARIS, PRIS\} \tag{27}$$

4 Optimizing Power Allocation in the ARIS-Assisted NOMA Spectrum-Sharing Systems

In this segment, we examine the optimization of power distribution to enhance the efficacy of the proposed ARIS-assisted NOMA spectrum-sharing framework. Initially, we ascertain the optimal power allocation coefficients at the BS (referred to as a_1^*) with the objective of individually minimizing the outage probability within the ARIS-NOMA network. This endeavor concentrates on determining the power allocation coefficients of a_1^* at the BS that yield the minimal outage probability. To accomplish this, we establish the ensuing minimization problems

$$\min_{a_1} \mathcal{P}^{\star}_{U_i}(a_1) \quad s.t. \begin{cases} a_1 + a_2 = 1 \\ a_1 < 0.5 \end{cases} \tag{28}$$

here, $\star \in \{ARIS, PRIS\}$ and $i \in \{1, 2\}$.

The objective function delineated in (28) exhibits a joint concavity in a_1, as illustrated in Figure 5. In light of the derived outage probability expressions, it proves challenging to ascertain closed-form expressions for the optimal values of the power allocation factor a_1. Fortunately, one may employ low-complexity algorithms founded on the golden section search method to address this issue. For instance, in Algorithm 1, we delineate the procedures to ascertain the precise value of a_1^* that minimizes the outage probability for the second user. The accuracy of Algorithm 1 is predominantly contingent upon the specified step search interval Δ.

5 Numerical Results

In this section, we conduct a numerical assessment of our theoretical findings regarding the performance of outage probability. We establish the fading parameters as $m = m_{g_0} = m_{g_1} = m_{g_2} = m_{h_0}$. The results obtained from Monte Carlo simulations are averaged over 10^6 independent trials. The target rate is measured in bits per channel user and is succinctly referred to as BPCU. In the subsequent figures, we abbreviate "Ana." and "Sim." to represent analytical computation and Monte Carlo simulation, respectively. The other principal parameters are encapsulated in Table I. In addition, we defined exponential distribution random variables as $\lambda_{h_0} = 0.1$ and $\lambda_{g_0} = \lambda_{g_1} = \lambda_{g_2} = 0.5$.

Figure 2 shows the outage probability of the secondary network versus the power p of the BS with different numbers of RIS. Regarding the outage probability for the ARIS and PRIS cases, we have demonstrated that the outage performance in the ARIS case is always better than PRIS.

Algorithm 1: Optimization Algorithm to find a_1^* based on Golden section search [8]

Input : Initialize $\psi_{\min} = 0$, $\psi_{\max} = 0.5$, the golden section search $\varpi = \frac{\sqrt{5}-1}{2}$ and a stopping threshold $\Delta = 10^{-3}$.

Output: The optimal of a_1^* that minimum the outage performance $\mathcal{P}^{\star}_{U_i}(a_1^*)$, $\star \in \{ARIS, PRIS\}$.

repeat
  $\beta_1 = \psi_{\max} - (\psi_{\max} - \psi_{\min})\,\varpi$.
  $\beta_2 = \psi_{\min} + (\psi_{\max} - \psi_{\min})\,\varpi$.
  Obtain $\mathcal{P}^{\star}_{U_i}(\beta_1)$ and $\mathcal{P}^{\star}_{U_i}(\beta_2)$ from (8), (9), (13) and (14).
  if $\mathcal{P}^{\star}_{U_i}(\beta_1) < \mathcal{P}^{\star}_{U_i}(\beta_2)$ **then**
    Update: $\psi_{\max} \leftarrow \beta_2$
  else
    Update: $\psi_{\min} \leftarrow \beta_1$
  end
until $|\psi_{\max} - \psi_{\min}| < \Delta$
return The optimal of $a_1^* = (\psi_{\max} + \psi_{\min})/2$

Table I
Main Parameters for Our Simulations [9]

Parameters	Notation	Values
Power splitting factors	$\{a_1, a_2\}$	$\{0.2, 0.8\}$
Target rates SINR to decode x_1 and x_2	$\{R_1, R_2\}$	$\{1.5, 1.5\}$ BPCU
The fading parameter	m	0.5
The interference constraint at PU	ρ_Q	5 dB
The reflection coefficient of ARIS	β	5
The noise power of ARIS	N_{tn}	-30 dBm

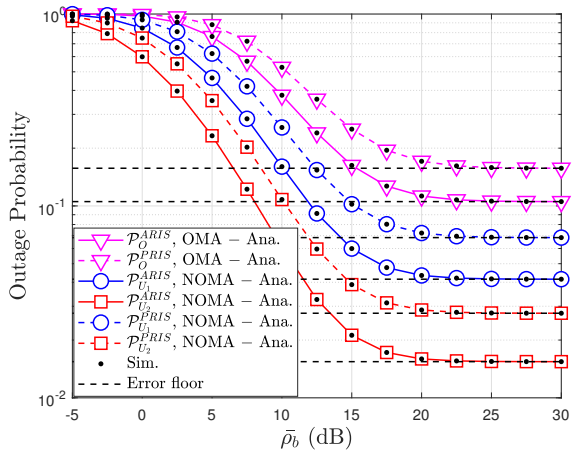

Figure 2. Outage probability versus the transmit power $\bar{\rho}_b$, with $N = 5$, $\beta = 5$, $m = 0.5$, $\rho_Q = 5$ [dB] and $R_1 = R_2 = 1.5$ [BPCU].

Figure 3 shows the outage probability versus the power $\bar{\rho}_b$ of the BS for different values of the channel and RIS numbers. From Figure 3 the outage probability of U_1 and U_2 is compared in the ARIS case. We can show the simulation compares outage performance

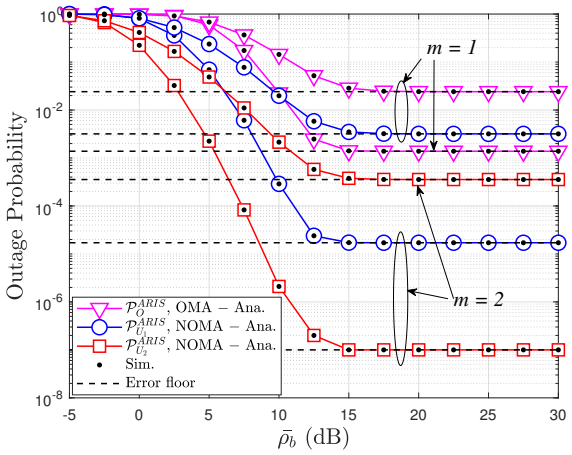

Figure 3. Outage probability versus the transmit power $\bar{\rho}_b$, with $N = 5$, $\rho_Q = 5$ [dB] and $R_1 = R_2 = 1.5$ [BPCU].

between OMA and NOMA, it is clear that the outage probability is improved when $N = 5, m = 2$.

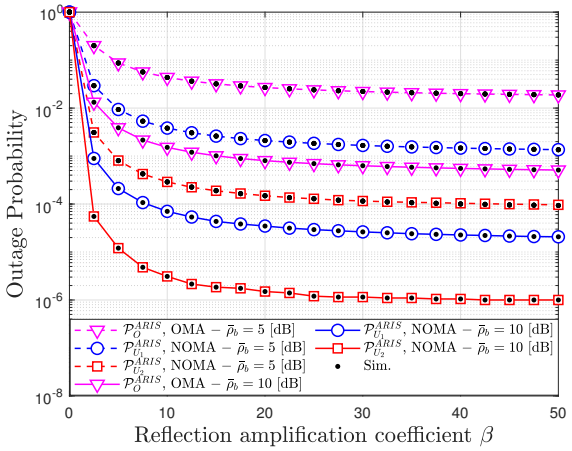

Figure 4. Outage probability versus the reflection amplitude factors β, with $N = 8$, $m = 0.7$, $\rho_Q = 10$ [dB] and $R_1 = R_2 = 1.5$ [BPCU].

Figure 4 illustrates the outage probability versus different reflection amplification coefficient β. We observe that the outage probability of the system improves as N increases with respect to the values of $\bar{\rho}_b$.

Figure 5 depicts the impact of power allocation factors from 0 to 0.3 based on the Golden Section search to optimize allocation factors on the system's outage probability. The Golden Search algorithm in Figure 5 can be applied with $a_1 = 0.3$.

Figure 6. The results show that the throughput of the system with ARIS-NOMA and PRIS-NOMA is not significantly different. The comparison results show that A/P RIS-NOMA outperforms A/P RIS-OMA in delay-limited systems. The resultant system throughput can be affected by the stochastic variations of the wireless channel. Figure 6 highlights the benefits of using NOMA in conjunction with ARIS to enhance system throughput compared to traditional OMA. It also illustrates the influence of transmit power and potentially different ARIS configurations on the overall system performance. The provided parameters offer

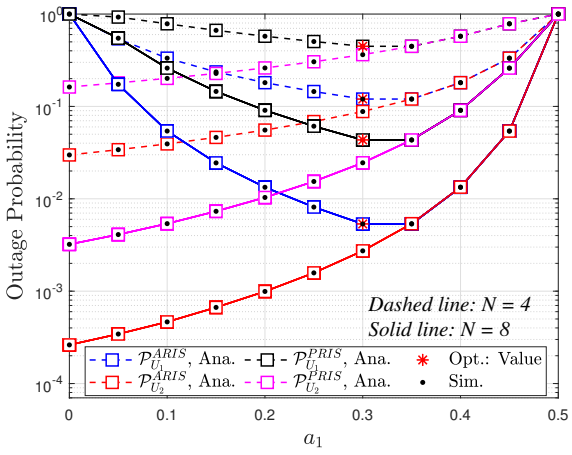

Figure 5. Outage probability versus power allocation factors, with $m = 0.5$, $R_1 = R_2 = 1$ [BPCU], $\rho_Q = 5$ [dB] and $\bar{\rho}_b = 5$ [dB].

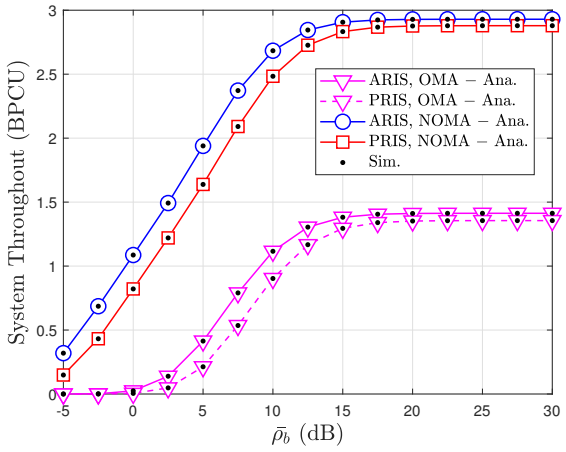

Figure 6. System throughput versus the transmit power $\bar{\rho}_b$, with $m = 0.7$, $R_1 = R_2 = 1.5$ [BPCU], $a_1 = 0.1$, $a_2 = 0.9$ and $\rho_Q = 5$ [dB].

specific context regarding the target rates and power allocation strategy within the NOMA scheme.

6 Conclusion

In this work, we proposed a novel RIS-assisted underlay spectrum sharing system, in which a secondary network assisted by an RIS shares the spectrum dedicated to a primary network. The performance of the RIS-assisted secondary network over Rician fading channels is investigated while considering a practical transmit power adaptation at the BS and an interference power constraint at the PR. Novel exact analytical expressions are derived to quantify the outage performance and throughput. The derived results suggest that increasing the number of RIS elements N will substantially enhance the performance of the secondary network. In addition, our analytical approach is validated through extensive Monte Carlo simulations.

Appendix A

Proof of Proposition 1 : In accordance with the definitions pertaining to outage probability for U_1, the

proof procedures commence by integrating (3) and (4) into (7), where $\mathcal{P}_{U_1}^{ARIS}$ is defined as follows

$$\begin{aligned} &P_{U_1}^{ARIS} = \\ &1-\Pr\left(\begin{array}{l}\left|\mathbf{g}_1^H\boldsymbol{\Theta}\mathbf{g}_0\right|^2 > \frac{\phi_2}{\rho_b}\left(\xi\beta N_{tn}\left|\mathbf{g}_1^H\boldsymbol{\Theta}\right|^2+1\right),\\ \left|\mathbf{g}_1^H\boldsymbol{\Theta}\mathbf{g}_0\right|^2 > \frac{\phi_1}{\rho_b}\left(\xi\beta N_{tn}\left|\mathbf{g}_1^H\boldsymbol{\Theta}\right|^2+1\right)\end{array}\right)\\ &=1-\Pr\left(\left|\mathbf{g}_1^H\boldsymbol{\Theta}\mathbf{g}_0\right|^2 > \frac{\phi_{\max}}{\rho_b}\left(\xi\beta N_{tn}\left|\mathbf{g}_1^H\boldsymbol{\Theta}\right|^2+1\right)\right), \end{aligned} \tag{29}$$

where $\phi_2 = \frac{\gamma_{th_2}}{\beta\left(a_2-\gamma_{th_2}a_1\right)}$, $\phi_1 = \frac{\gamma_{th_1}}{\beta a_1}$, $\phi_{\max} = \max\left(\phi_1,\phi_2\right)$. It is noted that $\rho_b = \min\left(\bar{\rho}_b, \frac{\rho_Q}{|h_0|^2}\right)$ in which $\bar{\rho}_b = \bar{P}_b/\sigma^2$ and $\rho_Q = Q/\sigma^2$, (29) is calculated as

$$\mathcal{P}_{U_1}^{ARIS} = 1-\mathcal{A}_1-\mathcal{A}_2. \tag{30}$$

Here, $\mathcal{A}_1$ and $\mathcal{A}_2$ are calculated below as follows

$$\begin{aligned} \mathcal{A}_1 =& \Pr\left(\begin{array}{l}\left|\mathbf{g}_1^H\boldsymbol{\Theta}\mathbf{g}_0\right|^2 > \frac{\phi_{\max}}{\bar{\rho}_b}\left(\xi\beta N_{tn}\left|\mathbf{g}_1^H\boldsymbol{\Theta}\right|^2+1\right),\\ |h_0|^2 < \frac{\rho_Q}{\bar{\rho}_b}\end{array}\right)\\ =& \Pr\left(\begin{array}{l}\left|\sum_{n=1}^N \left|g_0^n\right|\left|g_1^n\right|\right| > \sqrt{\frac{\phi_{\max}(d_1+1)}{\bar{\rho}_b}},\\ |h_0|^2 < \frac{\rho_Q}{\bar{\rho}_b}\end{array}\right)\\ =& F_{|h_0|^2}\left(\frac{\rho_Q}{\bar{\rho}_b}\right)\left[1-F_{\left|\sum\limits_{n=1}^N g_0^n g_1^n\right|}\left(\sqrt{\frac{\phi_{\max}n_1}{\bar{\rho}_b}}\right)\right], \end{aligned} \tag{31}$$

and

$$\begin{aligned} \mathcal{A}_2 =& \Pr\left(\begin{array}{l}\left|\mathbf{g}_1^H\boldsymbol{\Theta}\mathbf{g}_0\right|^2 > \frac{\phi_{\max}|h_0|^2}{\rho_Q}\left(\xi\beta N_{tn}\left|\mathbf{g}_1^H\boldsymbol{\Theta}\right|^2+1\right),\\ |h_0|^2 > \frac{\rho_Q}{\bar{\rho}_b}\end{array}\right)\\ =& \Pr\left(\begin{array}{l}\left|\sum_{n=1}^N \left|g_0^n\right|\left|g_1^n\right|\right| > \sqrt{\frac{\phi_{\max}(d_1+1)|h_0|^2}{\rho_Q}},\\ |h_0|^2 > \frac{\rho_Q}{\bar{\rho}_b}\end{array}\right)\\ =& \int_{\frac{\rho_Q}{\bar{\rho}_b}}^{\infty} f_{|h_0|^2}(x)\left[1-F_{\left|\sum\limits_{n=1}^N g_0^n g_1^n\right|}\left(\sqrt{\frac{\phi_{\max}d_1 x}{\rho_Q}}\right)\right]dx, \end{aligned} \tag{32}$$

where $d_1 = \xi\beta N_{tn}\Omega_1 + 1$. It is important to observe that the equation (31) has been formulated with the aid of coherent phase shifting, which serves to optimize the performance received by the intended users. In order to compute equation (31), it is imperative to first determine the PDF and CDF of the random variables $X = |h_0|^2$ and $Z = \sum_{n=1}^N \left|g_0^n\right|\left|g_1^n\right|$, respectively. Given that $|h_0|$ is presumed to conform to the Nakagami-m distribution, the associated PDF and CDF of X is represented as follows

$$f_{|h_0|^2}(x) = \frac{\mu_0^{m_0}x^{m_0-1}}{\Gamma(m_0)}e^{-\mu_0 x}, \tag{33a}$$

$$\begin{aligned} F_{|h_0|^2}(x) =& 1-\frac{\Gamma(m_0, x\mu_0)}{\Gamma(m_0)}\\ =& 1-e^{-\mu_0 x}\sum_{t=0}^{m_0-1}\frac{\mu_0^t x^t}{t!}, \end{aligned} \tag{33b}$$

where $\mu_0 = \frac{m_{h_0}}{\lambda_{h_0}}$ in which λ_{h_0} and m_{h_0} representing the mean and integer fading factor, respectively. It can be observed that the CDF of Z cannot be obtained through a direct method. Nevertheless, we may employ the Laguerre polynomials to furnish an estimated CDF. Let $Z_n = \left|g_0^n\right|\left|g_1^n\right|$, the expected value and variance of Z_n can be respectively expressed as $\mu_1 = \mathbb{E}\{Z_n\} = \frac{\Gamma\left(m_{g_0}+0.5\right)\Gamma\left(m_{g_1}+0.5\right)\sqrt{\lambda_{g_0}\lambda_{g_1}}}{\Gamma\left(m_{g_0}\right)\Gamma\left(m_{g_1}\right)\sqrt{m_{g_0}m_{g_1}}}$ and $\Omega_1 = \mathbb{D}\{Z_n\} = \lambda_{g_0}\lambda_{g_1}\left\langle 1-\frac{1}{m_{g_0}m_{g_1}}\left[\frac{\Gamma\left(m_{g_0}+0.5\right)\Gamma\left(m_{g_1}+0.5\right)}{\Gamma\left(m_{g_0}\right)\Gamma\left(m_{g_1}\right)}\right]^2\right\rangle$ in which m_{g_0}, m_{g_1} and m_{g_2} are the *shape parameter*, indicating the severity o fading and λ_{g_0}, λ_{g_1} and λ_{g_0} are the *spread parameter* of the distribution. From [9], the approximate CDF and PDF of Z are obtained as

$$f_Z(x) \approx \frac{x^{b_1}e^{-\frac{x}{c_1}}}{c_1^{b_1+1}\Gamma(b_1+1)}, \tag{34a}$$

$$\begin{aligned} F_Z(x) \approx& \frac{\gamma\left(b_1+1, c_1^{-1}x\right)}{\Gamma(b_1+1)}\\ \approx& 1-\frac{\Gamma\left(b_1+1, c_1^{-1}x\right)}{\Gamma(b_1+1)}, \end{aligned} \tag{34b}$$

where $b_1 = \frac{N[\mathbb{E}\{Z_n\}]^2}{\mathbb{D}\{Z_n\}}-1$, $c_1 = \frac{\mathbb{D}\{Z_n\}}{\mathbb{E}\{Z_n\}}$, $\gamma(.,.)$ is the lower incomplete Gamma function and $\Gamma(.,.)$ is the upper incomplete Gamma function.

First, by substituting (34b) and (33b) into (31), $\mathcal{A}_1$ can be obtained as

$$\mathcal{A}_1 = \left[1-e^{-\frac{\mu_0\rho_Q}{\bar{\rho}_b}}\sum_{t=0}^{m_0-1}\frac{\mu_0^t\rho_Q^t}{t!\bar{\rho}_b^t}\right]\frac{\Gamma\left(b_1+1, c_1^{-1}\sqrt{\frac{\phi_{\max}d_1}{\bar{\rho}_b}}\right)}{\Gamma(b_1+1)}. \tag{35}$$

Finally, substituting (34b) and (33b) into (32), $\mathcal{A}_2$ is written as

$$\mathcal{A}_2 = \frac{\mu_0^{m_0}}{\Gamma(m_0)\Gamma(b_1+1)}\int_{\frac{\rho_Q}{\bar{\rho}_b}}^{\infty} x^{m_0-1}e^{-\mu_0 x}\Gamma\left(b_1+1, \vartheta_1\sqrt{x}\right)dx, \tag{36}$$

where $\vartheta_1 = c_1^{-1}\sqrt{\frac{\phi_{\max}d_1}{\rho_Q}}$. Based on (36), using $t = \sqrt{x}$, $\mathcal{A}_2$ can be calculated as

$$\begin{aligned} \mathcal{A}_2 =& \frac{2\mu_0^{m_0}}{\Gamma(m_0)\Gamma(b_1+1)}\int_{\sqrt{\frac{\rho_Q}{\bar{\rho}_b}}}^{\infty} t^{2m_0-1}e^{-\mu_0 t^2}\Gamma(b_1+1, \vartheta_1 t)\,dt\\ =& \frac{2\mu_0^{m_0}}{\Gamma(m_0)\Gamma(b_1+1)}\int_0^{\infty} t^{2m_0-1}e^{-\mu_0 t^2}H\left(\sqrt{\frac{\bar{\rho}_b}{\rho_Q}}t-1\right)\\ &\times\Gamma(b_1+1, \vartheta_1 t)\,dt, \end{aligned} \tag{37}$$

where $H(.)$ is heaviside step function. To solve the integral $\mathcal{A}_2$, we utilize the following transformations involving the Meijer G-function [[10], Chapter 8.4], [8]

$$\int_0^\infty x^{\lambda-1} G_{p,q}^{m,0}\left(\eta x \left| \begin{matrix} \mathbf{a}_p \\ \mathbf{b}_q \end{matrix} \right.\right) G_{p_2,q_2}^{m_2,n_2}\left(\theta x^h \left| \begin{matrix} \mathbf{c}_{p_2} \\ \mathbf{d}_{q_2} \end{matrix} \right.\right) G_{p_3,q_3}^{m_3,n_3}\left(\delta x^k \left| \begin{matrix} \mathbf{e}_{p_3} \\ \mathbf{f}_{q_3} \end{matrix} \right.\right) dx = \eta^{-\lambda} \times H_{q,p:p_2,q_2:p_3,q_3}^{0,m:m_2,n_2:m_3,n_3}\left(\begin{matrix} (1-\mathbf{b}_q-\lambda;h,k) \\ (1-\mathbf{a}_p-\lambda;h,k) \end{matrix} \middle| \begin{matrix} (\mathbf{c}_{p_2},1) \\ (\mathbf{d}_{q_2},1) \end{matrix} \middle| \begin{matrix} (\mathbf{e}_{p_3},1) \\ (\mathbf{f}_{q_3},1) \end{matrix} \middle| \frac{\theta}{\eta^h}, \frac{\delta}{\eta^k} \right). \tag{40}$$

$$e^{-\mu_0 t^2} = G_{0,1}^{1,0}\left(\mu_0 t^2 \left| \begin{matrix} - \\ 0 \end{matrix} \right.\right), \tag{38a}$$

$$H\left(\sqrt{\frac{\bar{\rho}_b}{\rho_Q}}t - 1\right) = G_{1,1}^{0,1}\left(\sqrt{\frac{\bar{\rho}_b}{\rho_Q}}t \left| \begin{matrix} 1 \\ 0 \end{matrix} \right.\right), \tag{38b}$$

$$\Gamma(b_1+1, \vartheta_1 t) = G_{1,2}^{2,0}\left(\vartheta_1 t \left| \begin{matrix} 1 \\ b_1+1, 0 \end{matrix} \right.\right), \tag{38c}$$

Plugging (38c), (38b) and (38a) into (37), $\mathcal{A}_2$ can be expressed as

$$\mathcal{A}_2 = \frac{2\mu_0^{m_0}}{\Gamma(m_0)\Gamma(b_1+1)} \int_0^\infty t^{2m_0-1} G_{0,1}^{1,0}\left(\mu_0 t^2 \left| \begin{matrix} - \\ 0 \end{matrix} \right.\right) \times G_{1,1}^{0,1}\left(\sqrt{\frac{\bar{\rho}_b}{\rho_Q}}t \left| \begin{matrix} 1 \\ 0 \end{matrix} \right.\right) G_{1,2}^{2,0}\left(\vartheta_1 t \left| \begin{matrix} 1 \\ b_1+1, 0 \end{matrix} \right.\right) dt. \tag{39}$$

We apply the following (40) to solve integrals (39) on the next top page in which $H_{p,q:u,v:e,f}^{m,n:s,t:i,j}(\cdot)$ stands for the extended generalized bivariate Fox H-function (EGBFHF) in [11]. This function can be conveniently evaluated using mathematical software such as Mathematica [[12], Table I] and Matlab [[13], Appendix A].

Base on (40), $\mathcal{A}_2$ is written as

$$\begin{aligned}\mathcal{A}_2 &= \frac{2\mu_0^{m_0}}{\Gamma(m_0)\Gamma(b_1+1)} \int_0^\infty t^{2m_0-1} G_{1,2}^{2,0}\left(\vartheta_1 t \left| \begin{matrix} 1 \\ b_1+1, 0 \end{matrix} \right.\right) \times G_{0,1}^{1,0}\left(\mu_0 t^2 \left| \begin{matrix} - \\ 0 \end{matrix} \right.\right) G_{1,1}^{0,1}\left(\sqrt{\frac{\bar{\rho}_b}{\rho_Q}}t \left| \begin{matrix} 1 \\ 0 \end{matrix} \right.\right) dt \\ &= \frac{2\mu_0^{m_0}\vartheta_1^{-2m_0}}{\Gamma(m_0)\Gamma(b_1+1)} \Lambda\left(\frac{\mu_0}{\vartheta_1^2}, \frac{1}{\vartheta_1}\sqrt{\frac{\bar{\rho}_b}{\rho_Q}}\right).\end{aligned} \tag{41}$$

where $\Lambda(a,b,c)$ is already given below (9). Substituting (41) and (35) into (30), we can obtain (8).

The proof is completed.

References

[1] J. Li, L. Yang, Q. Wu, X. Lei, F. Zhou, F. Shu, X. Mu, Y. Liu, and P. Fan, "Active RIS-Aided NOMA-Enabled Space- Air-Ground Integrated Networks With Cognitive Radio," *IEEE Journal on Selected Areas in Communications*, vol. 43, no. 1, pp. 314–333, 2025.

[2] P. T. Tin, M.-S. V. Nguyen, D.-H. Tran, C. T. Nguyen, S. Chatzinotas, Z. Ding, and M. Voznak, "Performance Analysis of User Pairing for Active RIS-Enabled Cooperative NOMA in 6G Cognitive Radio Networks," *IEEE Internet of Things Journal*, vol. 11, no. 23, pp. 37 675–37 692, 2024.

[3] M. Shen, L. Li, and X. Lei, "Robust Beamforming for Active Reconfigurable Intelligent Surface-Aided Secure CR-NOMA Systems," *IEEE Transactions on Vehicular Technology*, vol. 73, no. 12, pp. 18 748–18 754, 2024.

[4] B. Zheng, C. You, W. Mei, and R. Zhang, "A Survey on Channel Estimation and Practical Passive Beamforming Design for Intelligent Reflecting Surface Aided Wireless Communications," *IEEE Communications Surveys and Tutorials*, vol. 24, no. 2, pp. 1035–1071, 2022.

[5] P. Mittal and K. Gupta, "An integral involving generalized function of two variables," in *Proceedings of the Indian academy of sciences-section A*, vol. 75, no. 3. Springer, 1972, pp. 117–123.

[6] Y. Pei, X. Yue, W. Yi, Y. Liu, X. Li, and Z. Ding, "Secrecy outage probability analysis for downlink RIS-NOMA networks with on-off control," *IEEE Transactions on Vehicular Technology*, vol. 72, no. 9, pp. 11 772–11 786, 2023.

[7] V. S. Adamchik and O. Marichev, "The algorithm for calculating integrals of hypergeometric type functions and its realization in REDUCE system," in *Proceedings of the international symposium on Symbolic and algebraic computation*, 1990, pp. 212–224.

[8] D.-T. Do, C.-B. Le, A. Vahid, and S. Mumtaz, "Antenna selection and device grouping for spectrum-efficient UAV-assisted IoT systems," *IEEE Internet of Things Journal*, vol. 10, no. 9, pp. 8014–8030, 2022.

[9] X. Yue, M. Song, C. Ouyang, Y. Liu, T. Li, and T. Hou, "Exploiting active RIS in NOMA networks with hardware impairments," *IEEE Transactions on Vehicular Technology*, vol. 73, no. 6, pp. 8207–8221, 2024.

[10] A. Prudnikov, *Integrals and series*. Routledge, 2018.

[11] P. Mittal and K. Gupta, "An integral involving generalized function of two variables," in *Proceedings of the Indian academy of sciences-section A*, vol. 75, no. 3. Springer, 1972, pp. 117–123.

[12] H. Lei, I. S. Ansari, G. Pan, B. Alomair, and M.-S. Alouini, "Secrecy capacity analysis over $\alpha-\mu$ fading channels," *IEEE Communications Letters*, vol. 21, no. 6, pp. 1445–1448, 2017.

[13] K. P. Peppas, "A new formula for the average bit error probability of dual-hop amplify-and-forward relaying systems over generalized shadowed fading channels," *IEEE Wireless Communications Letters*, vol. 1, no. 2, pp. 85–88, 2012.

Hong-Nhu Nguyen is currently a lecturer at Saigon University, Ho Chi Minh City, Vietnam. His research interests include applied electronics, wireless communications, cognitive radio, NOMA, and energy harvesting. He can be contacted at email: nhu.nh@sgu.edu.vn.

Ngoc Thuy Trang Nguyen is currently a student for 3 years at the Faculty of Electronics and Telecommunications, Saigon University (SGU), Ho Chi Minh City, Vietnam. She can be contacted at email: 3122500042@sv.sgu.edu.vn.

Hai Sinh Chu is currently a student for 3 years at the Faculty of Electronics and Telecommunications, Saigon University (SGU), Ho Chi Minh City, Vietnam. He can be contacted at email: 3122500032@sv.sgu.edu.vn.

Nguyen Minh Quan Bui is currently a student for 3 years at the Faculty of Electronics and Telecommunications, Saigon University (SGU), Ho Chi Minh City, Vietnam. He can be contacted at email: 3122520036@sv.sgu.edu.vn.